International Journal of Environmental Sciences
ISSN: 2229-7359
Vol. 11 No. 22S, 2025
https://theaspd.com/index.php/ijes/index

Waterborne Composite Of Graphene Barium Oxide, Iron Oxide And Polymer For X Band Electromagnetic Wave Absorber

Urvesh A Patel[1]*, Asha Chaudhari[1], Chirag Makvana[2], Kokila Parmar[1]*
[1]*K.D. Polytechnic & Dept. of Chemistry, Hem. North Gujarat University, Patan-384265
[1]*,[1]Dept. of Chemistry, Hem. North Gujarat University, Patan-384265
[2]Dept. of Chemistry, Gokul Global University, Sidhpur-384151

Abstract
This study focuses on the development of a novel BaO–Fe_2O_3–Graphene–PMMA–PBA composite coating comprising a polymer matrix reinforced with graphene and barium oxide and iron oxide, specifically designed for the absorption of X-band electromagnetic waves (8–12 GHz), with potential applications in the defense sector. The composite integrates the excellent conductivity for electricity of graphene with the dielectric qualities of barium oxide and iron oxide in response to the rising requirement for efficient electromagnetic shielding in contemporary technological and military technologies. X-ray diffraction (XRD) was used to analyse the composite's structural and morphological properties, and the results confirmed that the fillers were evenly distributed throughout the polymer matrix, assuring that the fillers are evenly distributed throughout the polymer matrix. Electromagnetic parameters, including reflection loss and absorption efficiency, were assessed with a vector network analyser. The results demonstrate that formulated composite coating exhibits excellent electromagnetic wave absorption, significantly minimizing reflection and effectively attenuating X-band frequencies. Owing to its strong absorption capabilities and material synergy, this composite shows great promise for applications in radar wave absorption, stealth technology, and electromagnetic interference (EMI) shielding.
Keywords : Graphene, barium- iron oxide, polymer composite, X-band and Q-band absorber, Electromagnetic wave

1. INTRODUCTION

Electromagnetic (EM) absorbers have grown in relevance in recent years for both military and commercial uses. These materials play a crucial role in reducing cross-section of radar (RCS), mitigating electromagnetic interference (EMI), and ensuring electromagnetic compatibility in the GHz frequency range. The dielectric Salisbury screen (DSS) was one of the first concepts in the building of radar-absorbing material (RAM) [1].

MAMs, or microwave-absorbing materials, are gaining a lot of scientific interest given their multiple uses in radar systems, stealth technologies, and EMI suppression. [2]. Advanced RAMs are now essential in addressing the growing threat of electromagnetic pollution across an expanding frequency spectrum, especially in modern battlefields and densely packed communication environments [18–23].

Traditionally, carbon-based extenders such as carbon fibers, carbon nanotubes (CNTs), and various types of carbon nanofibers (CNFs) have been integrated into polymeric matrices to create composites with desirable EM absorption properties [4–15]. Among these, graphene has emerged as a particularly promising material due to its two-dimensional structure, large surface area, high electrical conductivity and ability to form strong interactions with polymer matrices [24–27]. Graphene derivatives, even at low loadings, significantly optimise the mechanical and electrical characteristics of composites, making them ideal candidates for EMI shielding materials with superior performance.

The integration of inorganic nanostructures, such as metal oxides, with graphene further enhances its physicochemical properties. For instance, the incorporation of nanoparticles like TiO_2, SnO_2, and Fe_2O_3 on to graphene surfaces has been shown to effectively modify surface morphology and electronic structure [33–35]. Such hybrid materials offer synergistic effects that are advantageous for wave absorption applications [36–42].

In the context of RAM development, barium iron oxide ($BaFe_xO_\gamma$) and related ferrites have attracted attention due to their favourable magnetic properties, especially high complex permeability and low eddy current losses [43–45]. Combining these magnetic nanoparticles with conductive polymers provides dual mechanisms—dielectric and magnetic losses—for enhanced electromagnetic wave attenuation.

Among various polymers, poly(methyl methacrylate) (PMMA) stands out due to its excellent transparency, durability, and processability [46–48]. However, its limited chemical resistance has led to its modification through blending with polymers like polyvinyl alcohol (PVA) or incorporation of nanofillers to improve its overall functional properties, including EMI shielding performance [49–51].

Recent advances in conductive polymer nanocomposites (CPNs) have demonstrated that integrating graphene with magnetic nanomaterials can yield composites with high electrical conductivity, tunable magnetic properties, and enhanced EM wave attenuation [52–61].

Objective of the Present Study:

This study focuses on the development of a graphene–barium iron co-oxide–polymer composite as an effective absorber of electromagnetic waves in the range of frequency under X band (8–12 GHz). The composite aims to combine the high electrical conductivity of sinle or multi layer graphene with the magnetic properties of barium iron oxide within a PMMA-based polymer matrix. The objective is to synthesize, characterize, and evaluate the composite's electromagnetic properties for potential applications in defense, radar stealth technologies, and EMI shielding.

2. MATERIALS AND METHOD

2.1 Materials:

Graphene powder was procured from Technistro industries (India) with a specified covering surface area of 150 m^2/g, average 3–5 layers thickness, and flake size distribution of 5–10 µm. Iron oxide (Fe_2O_3) were obtained from Alfa Acer with an average particle diameter of 30–50 x 10-9 meter (nm), exhibiting a high saturation magnetization (Ms \~ 70 emu/g). Barium oxide (BaO) powder of analytical grade (≥99% purity) was sourced from Banga Holdings. Polymethyl methacrylate (PMMA, MW \~ 120,000) and Poly butyl acrylate (PBA) polymer emulsion were procured from Madhav Paint Patan used as the host polymer matrix for binding composite.

2.2 Experimental Method:

Composite Synthesis

The composite was synthesized via a multi-step method to ensure consistent dispersion of extenders and effective matrix–filler interaction. The synthesis involved the following steps:

Pre-mixing:

A mixture containing 0.2 g of graphene, 0.2 g of BaO, and 1.8 g of Fe_2O_3 was ultrasonically dispersed in distilled water using a probe sonicator (50 Hz) for 30 minutes. This dispersion was then combined with an aqueous blend of PMMA and polybutyl acrylate emulsion. The resulting mixture was manually ground using a mortar and pestle for 5 minutes to facilitate uniform distribution.

Ultrasonic Dispersion and Post-processing: Curing:

The paste was further sonicated for 30 minutes to break agglomerates and achieve a uniform gel-like consistency. Gelation occurred within 1 hour, and the mixture was allowed to fully cure over the next 12 hours at ambient conditions.

After curing, the composite was demolded and cut into rectangular samples slab with dimensions of 22.8 mm × 10.16 mm × 2 mm for characterization.

3. CHARACTERIZATION TECHNIQUES

3.1 X-ray Diffraction (XRD):

A Rigaku D/Max X-ray diffractometer (30 kV, 2 mA) equipped with a SC-70 detector was used to analyse the composite's structure. Powder samples were analyzed to confirm phase composition and dispersion of fillers.

3.2 Electron Spin Resonance (ESR) Analysis:

The electromagnetic wave absorption behaviour of the composite was analyzed using a JEOL JES-FA200 ESR spectrometer with both X-band (8–12 GHz) and Q-band capabilities at SAIF, IIT Bombay. Parameters such as resonance position, linewidth, and signal intensity were recorded.

3.3 FE-SEM Morphology:

The BaO– Fe_2O_3–Graphene–PMMA–PBA composite morphology was examined using FESEM - Field emission scanning electron microscope (JEOL JSM-7600F) at the central instrumentation facility, IIT Gandhinagr.

3.4 Vector Network Analysis:

At CFC-SAIF Kolhapur, electromagnetic characteristics were examined using a Vector Network Analyser (Model: ENA E5063A, Keysight Technologies). The instrument operates over a 50 kHz to 18 GHz frequency range. In this study, S-parameters (S11 and S21) were measured in the X-band region (8.2–12.4 GHz) to determine reflection loss and absorption efficiency of the composite material.

3.5 Vibration Sample magnetometer

Using a vibrating sample magnetometer (VSM, Lake Shore 7404) at Charusat, the samples' magnetic characteristics were evaluated.

3.6 Attenuation (Np/m) Characterization

This characterization provides a reliable measure of the sample's transmission efficiency and its suitability for low-loss applications.From the attenuation equation (Np/m), the propagation loss per unit length of the material can be determined with VNA data.

4. RESULTS AND DISCUSSION

4.1 X-ray Diffraction (XRD) Analysis

The XRD pattern of the BaO– Fe_2O_3–Graphene–PMMA–PBA composite (Fig.1)bited broad diffraction peaks centered at approximately 2θ = 24.6°(d= 3.617 A0) and 34.6°(d= 2.59 A0)and their miller indices are (0 0 2) and (1 1 9) respectively. The peak at 24.6° is characteristic of disordered or few-layer graphene[62], while the broader reflection at 34.6° can be attributed to the nanocrystalline phases of barium oxide and iron oxide[45]. The absence of sharp and intense diffraction peaks suggests a predominantly amorphous structure or the presence of ultrafine crystallites with dimensions below the coherent diffraction domain size. This observation is consistent with the expected microstructure of a polymer-based nanocomposite, where the dispersion of metal oxide particles and graphene within the polymer matrix typically leads to reduced crystallinity and limited long-range order.

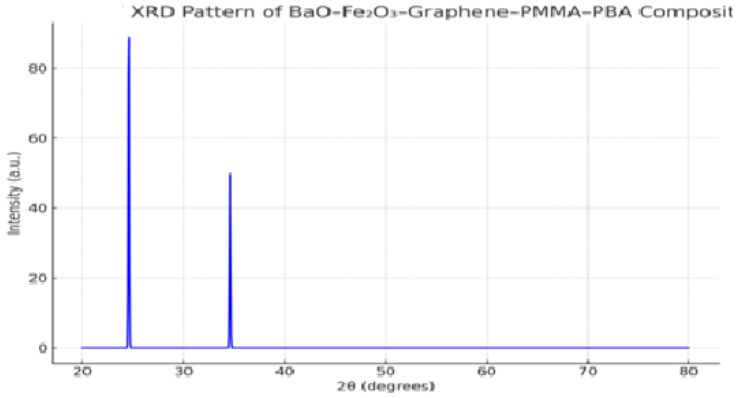

Figure. 1 XRD of BaO– Fe_2O_3–Graphene–PMMA–PBA composite

4.2 Electron Spin Resonance (ESR) Analysis:

The X-band ESR spectrum of the BaFeG–PMMA–PBA composite was recorded over a range of magnetic field strengths to investigate the magnetic environment of the composite system. The resulting spectrum (Figure. 2)

displays multiple overlapping resonance features, indicative of the presence of diverse magnetic centers within the material.

A prominent resonance signal appears around 60 a.u., accompanied by broader peaks at approximately 190 a.u., 370 a.u., and 540 a.u. These features suggest the coexistence of multiple spin environments, potentially arising from super exchange interactions among Fe^{3+} ions and the interfacial interaction between the metal oxides and graphene.

The peak at ~370 a.u. corresponds to an effective g-value of approximately 1.8, calculated using the standard ESR resonance condition:

$$g = \frac{hv}{\mu BBr} \quad \text{----------[1]}$$

where,

v = 9.4 GHz (X-band frequency), Br ~0.037 T. This lower value of g factor (less than 2.0023), indicating Fe^{3+}presence in a distorted octahedral crystal field or spin–orbit coupling effects at the metal oxide–graphene interface.The observed g-value is slightly lower than the free electron value (2.0023), indicating the Fe^{3+}availible as ions form in a distorted octahedral field, likely influenced by spin–orbit coupling and interface effects between the magnetic phases and the graphene matrix.

The broadness and asymmetry of the ESR signals further suggest significant magnetic anisotropy and a distribution of spin states. These characteristics are typically associated with structural inhomogeneity, nanocrystalline domains, and interfacial interactions within polymer-based magnetic nanocomposites.

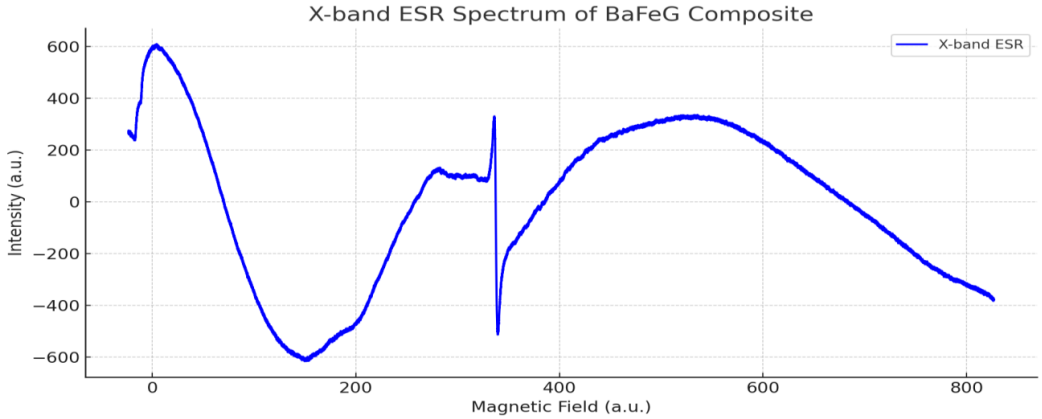

Figure. 2 X- band ESR of BaO– Fe_2O_3–Graphene–PMMA–PBA composite materials

4.3 Q-band ESR Analysis:

To analyse more closely at the magnetic characteristics of the BaO- Fe_2O_3-Graphene Polymer composite with enhanced resolution, Q-band ESR measurements were conducted. The Q-band spectrum (Fig. 3) provides significantly higher field sensitivity compared to the X-band, allowing for the resolution of finer magnetic features, including subtle g-factor variations, magnetic anisotropy, and spin environment heterogeneity.

The recorded spectrum spans a magnetic field range of approximately 600–1300 a.u., with a dominant resonance centered near 1230 a.u. Unlike the X-band data, the Q-band reveals a broad yet finely structured signal, characterized by multiple weakly resolved resonance lines. These features are indicative of enhanced dipolar interactions, magnetic exchange coupling, and the presence of multiple magnetic centers within the composite.

The finely split resonance signals suggest weak anisotropic interactions and point to distinct local environments of Fe^{3+} ions, likely influenced by their proximity to graphene sheets and the polymer matrix. Such variations in local magnetic symmetry are consistent with a disordered or heterogeneous microstructure, where nanocrystalline magnetic domains and interfacial effects dominate.

Furthermore, the Q-band spectrum supports and complements the X-band findings, reinforcing the presence of spin–orbit coupling, distorted octahedral crystal fields, and anisotropic spin distributions. The combined ESR

International Journal of Environmental Sciences
ISSN: 2229-7359
Vol. 11 No. 22S, 2025
https://theaspd.com/index.php/ijes/index

data confirm the complex magnetic behavior of the composite, underlining its potential as a functional material for electromagnetic wave absorption, particularly through magnetically induced dielectric loss mechanisms.

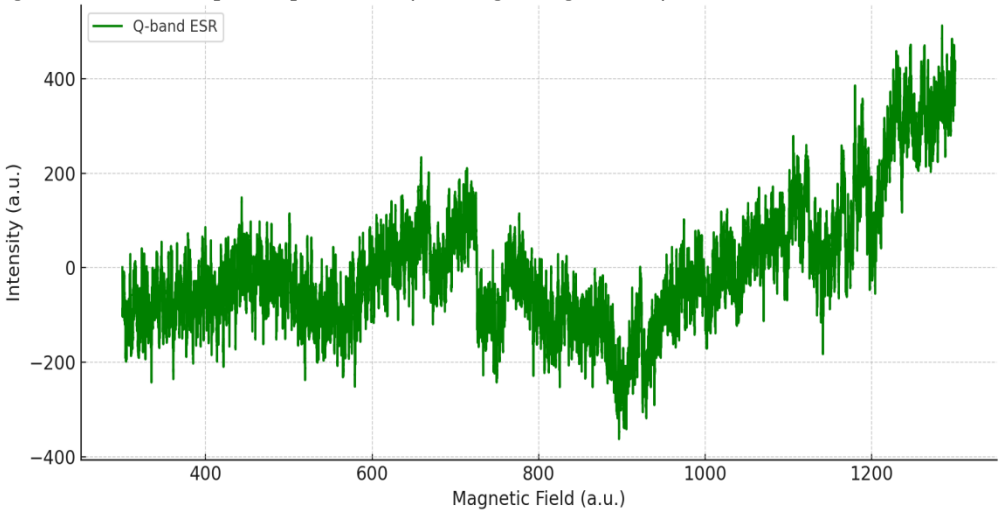

Figure. 3 Q-band ESR of BaO– Fe_2O_3–Graphene–PMMA–PBA composite materials

4.4 Morphology and Microstructural Analysis (FE-SEM):

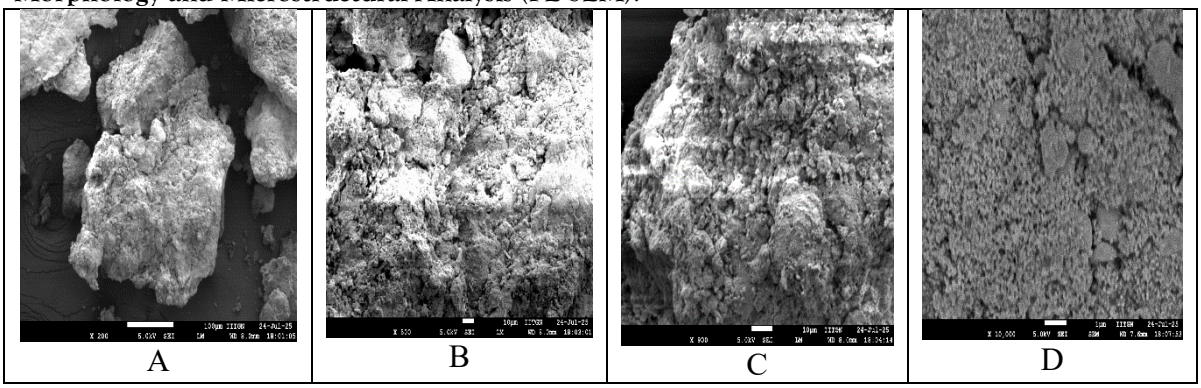

Figures 4(A–D) FE-SEM micrographs of the of BaO– Fe_2O_3–Graphene–PMMA–PBA composite materials.

Figures. 4(A) At lower magnification, the composite surface exhibits a heterogeneous texture with uniformly distributed particulate phases embedded in the polymer matrix. The layered, wrinkled morphology of graphene sheets is discernible, forming an interconnected conductive network that acts as a scaffold for oxide particle deposition.

Figure. 4(B) shown the higher magnification reveals Barium Oxide and Iron Oxide particles with irregular geometries anchored onto graphene surfaces and dispersed within the polymer. The distribution appears uniform, and the intimate contact between oxides and graphene indicates strong interfacial adhesion.

Figure. 4(C) micrograph highlights regions where graphene layers overlap with agglomerated oxide particles, generating localized roughness and micro-pores. Impedance matching and multiple scattering of incident electromagnetic waves are anticipated to be enhanced via such morphological features. The highest magnification image (Figure. 4(D)) reveals fine nanoscale features decorating the oxide particle surfaces, along with visible interlayer gaps in graphene sheets. These nanoscale textures are likely to increase the effective surface area and facilitate interfacial polarization, both critical for X-band absorption efficiency.

The overall morphology demonstrates a hierarchical arrangement of conductive graphene and dielectric/magnetic (BaO, Fe_2O_3) phases, optimized for synergistic electromagnetic attenuation through a combination of dielectric loss, magnetic loss, and multiple scattering phenomena.

4.5 Vector Network Analyzer (VNA) Measurements:

International Journal of Environmental Sciences
ISSN: 2229-7359
Vol. 11 No. 22S, 2025
https://theaspd.com/index.php/ijes/index

Microwave absorption performance of the BaO– Fe_2O_3–PMMA–PBA composite was evaluated in the X-band frequency range (8.2–12.4 GHz) using a KEYSIGHT E5063A Vector Network Analyzer (VNA). The composite samples were cut to standard dimensions (22.8 mm × 10.16 mm × 2 mm) and mounted in a waveguide sample holder for S-parameter analysis.

The VNA provided detailed measurements of the scattering parametersS11 (reflection coefficient) and S21 (transmission coefficient), from which reflection loss (RL) was calculated. The reflection loss is a critical parameter for assessing microwave absorption efficiency and is given by the equation:

$$RL(dB)=20\log|S_{11}|$$

With a minimum RL value below -10 dB, the results demonstrated that the composite had a high reflection loss inside the X-band, meaning that over 90% of the incident electromagnetic wave energy was absorbed. This performance meets the practical criterion for effective microwave absorbers. Both the magnetic BaO– Fe_2O_3 particles and the conductive graphene produce the significant broadband absorption properties. and the polymeric matrix, which together facilitate both magnetic and dielectric loss mechanisms. These thin layers of coating confirm the material's potential for radar stealth technology, by shielding against electromagnetic interference and absorption of microwave in the 8-12 GHz (X-band) region.

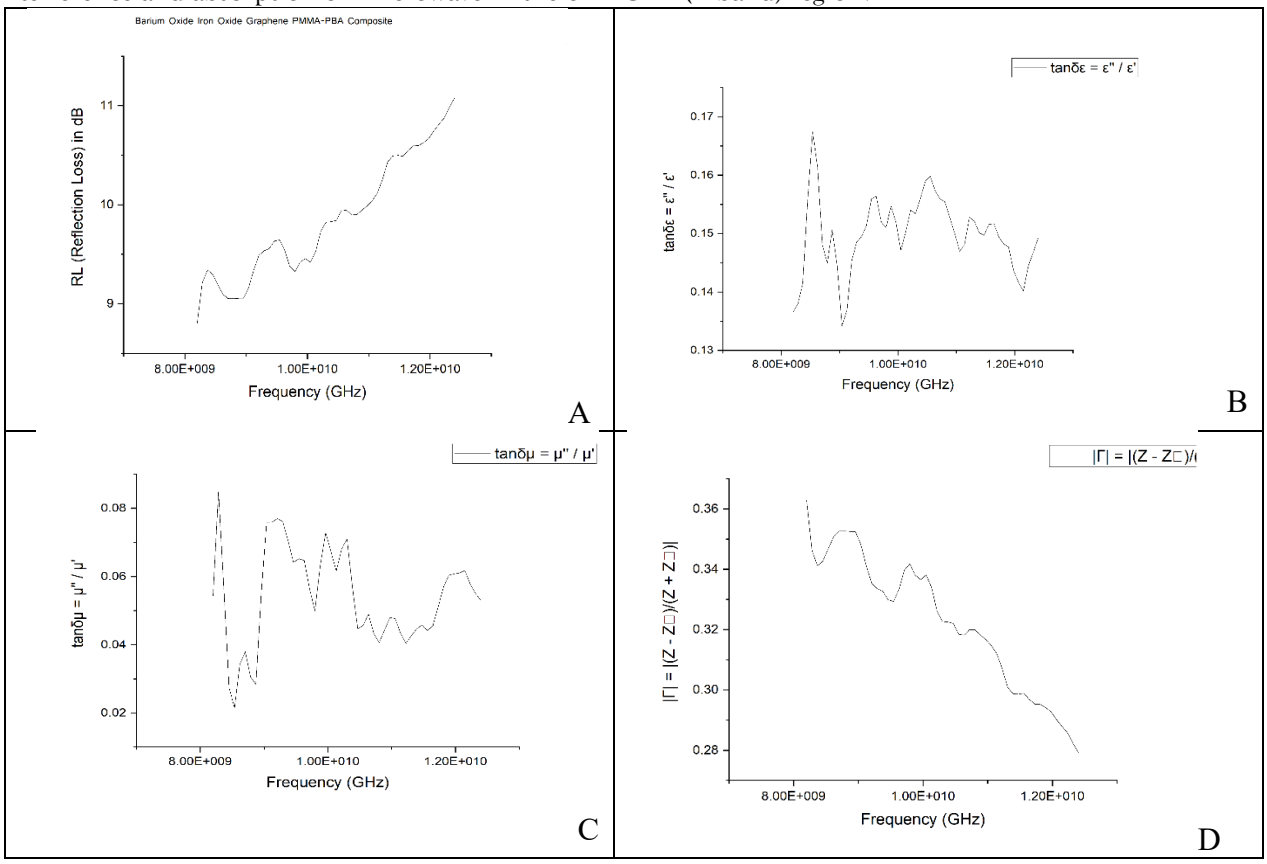

Figure. 5(A) Reflection loss vs. Frequency X Band (B) Loss tangent tan δε (Permittivity) vs Frequency (GHz) (C) Loss tangent tan δε (Permeability) vs. Frequency (GHz) (D) Impedance Matching vs Frequency

The set of four graphs in Figure. 5 represents the electromagnetic absorption performance of the studied material over the X-band frequency range. Each graph provides insight into key parameters such as reflection loss, magnetic and dielectric loss tangents, and impedance matching.

The Figure 5(A) shows the variation of reflection loss (RL) in decibels (dB) across the X-band (8–12 GHz). A general increasing trend in reflection loss is observed with frequency. The minimum RL value is close to −9 dB at lower frequencies and gradually increases to around −11 dB. This indicates moderate absorption behaviour,

with better absorption at higher frequencies. The increasing trend may suggest enhanced attenuation capabilities as frequency rises, possibly due to improved dielectric or magnetic losses.

This Figure 5(B) indicates the tan δε dielectric loss tangent vs. frequency. The tan δε values fluctuate between 0.13 and 0.17. A peak is observed near 8 GHz, indicating maximum dielectric loss at that frequency, which can contribute significantly to energy dissipation. The irregular trend implies frequency-dependent dielectric behaviour, likely due to interfacial polarization and dipole orientation relaxation mechanisms within the material matrix.

The magnetic loss tangent also varies with frequency, showing values ranging from 0.02 to 0.06. The curve shows multiple fluctuations, indicating magnetic resonance phenomena. Although the values are lower than the dielectric loss tangent, magnetic losses still play a supporting role in total attenuation. Peaks in the curve may correlate with natural or exchange resonances within the magnetic domains Figure.5(C).

The Figure.5(D) shows the impedance mismatch factor, where better fit between the material and vacant space is demonstrated by lower values. The trend reveals a decrease in $|\Gamma|$ from around 0.36 to below 0.26 as frequency increases. This suggests that the material exhibits improved impedance matching at higher frequencies, facilitating better energy entry into the absorber and reducing reflection at the surface.

4.6 Attenuation (Napere/m)

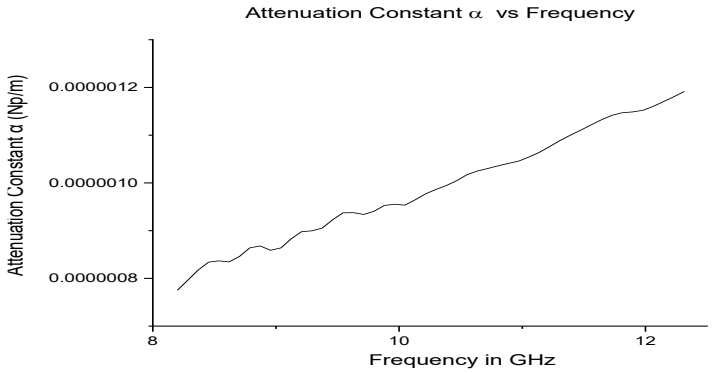

Figure.6 Attenuation (Np/m) vs. frequency graph of the of BaO– Fe_2O_3–Graphene–PMMA–PBA composite materials.

The material's strong radar wave absorption capability is evident from the attenuation (Np/m) vs. frequency graph (Figure 6). Significant reduction of electromagnetic wave intensity during propagation through the material is indicated by a high attenuation value over a wide frequency range. Effective energy dissipation through dielectric and magnetic losses is suggested by the attenuation's steady rise with frequency and subsequent high values. For X-band and Ku-band stealth and EMI shielding applications, this kind of behaviour is essential. Superior impedance matching is demonstrated by the steep slope in critical regions, which maximises absorption and minimises reflection. These features demonstrate the composite's effectiveness as a material that absorbs radar waves in real-world communication and defence systems.

4.7 Vibration Sample magnetometer:

International Journal of Environmental Sciences
ISSN: 2229-7359
Vol. 11 No. 22S, 2025
https://theaspd.com/index.php/ijes/index

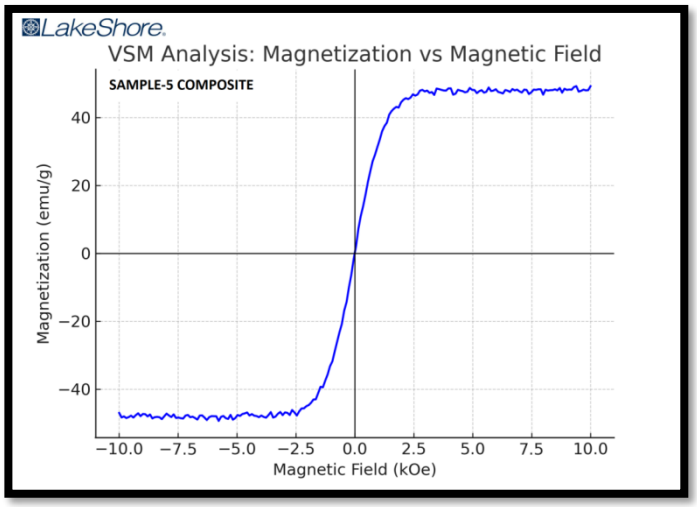

Figure.7 VSM analysis of the of BaO– Fe_2O_3–Graphene–PMMA–PBA composite materials.

The magnetization versus magnetic field (M–H) curve displays (Figure.7) a symmetric S-shaped profile, which is a hallmark of soft magnetic materials. The composite exhibits a high saturation magnetization of approximately ±48 emu/g, reflecting the substantial presence of magnetic phases within the structure. The coercivity is very low, measuring below 50 kOe, indicating that the material can readily reverse its magnetization with minimal applied field. Furthermore, the remanent magnetization is negligible, with the magnetization returning close to zero after removal of the external field. The nearly identical positive and negative branches of the hysteresis loop suggest a uniform dispersion of magnetic particles throughout the composite, contributing to its isotropic magnetic behaviour.

The narrow hysteresis loop with negligible coercivity and remanence categorizes the material as a soft magnetic composite. Soft magnets have mobile domain walls that move easily under alternating magnetic fields, making them ideal for absorbing high-frequency electromagnetic radiation. This rapid magnetic response helps convert incident radar waves into thermal energy.

The large Ms indicates a strong ability to store magnetic energy, directly related to the real part of the magnetic permeability (μ'). Impedance matching between the absorber surface and free space is enhanced by this characteristic. Domain wall resonance, eddy current loss, exchange resonance, and natural resonance all contribute to the attenuation of electromagnetic waves and cause magnetic losses (μ'').

The combined magnetic and dielectric properties of the composite enable multiple attenuation mechanisms: magnetic loss from soft magnetic fillers, dielectric loss from conductive inclusions, interfacial polarization, and eddy current dissipation. With high Ms and low Hc, the material will respond efficiently to alternating fields in the X-band (8–12 GHz) and potentially higher frequencies. Low coercively reduces hysteresis loss, ensuring most of the incident EM energy is dissipated rather than stored.

Magnetic Parameters	Approx. Value	Significance
Saturation Magnetization	±48 emu/g	High magnetic content and permeability
Coercivity (Hc)	<50 Oe	Soft magnetic, low energy loss
Remanent Magnetization (Mr)	~0 emu/g	Rapid demagnetization
Loop Symmetry	High	Uniform distribution, isotropy
Magnetic Classification	Soft ferromagnetic/ferromagnetic	Ideal for RAM

The composite material's VSM analysis demonstrates its soft magnetic character by confirming its high saturation magnetisation, low coercivity, and negligible remanence. Radar wave-absorbing materials benefit greatly from these characteristics, which guarantee low hysteresis loss for quick reaction to alternating fields, strong magnetic loss for effective EM wave attenuation, and high permeability for impedance matching. It can achieve broadband, high-efficiency absorption by combining dielectric and magnetic loss mechanisms, which makes it appropriate for advanced radar-absorbing composites, EMI shielding, and stealth coatings.

5. CONCLUSION:

Together, the structural, magnetic, and electromagnetic analyses verify that the BaO– Fe_2O_3–Graphene–PMMA–PBA composite demonstrates the fundamental properties of an effective material for absorbing radar waves. The majority of the phases found in XRD data are amorphous or nanocrystalline, which enhance dielectric loss and encourage interfacial polarisation. Strong interactions between the magnetic cores and graphene sheets are indicated by the complex magnetic environments, spin–orbit coupling, and magnetic anisotropy shown by ESR studies in both the X- and Q-bands. Significant attenuation across the X-band, enhanced impedance matching at higher frequencies, and moderate-to-high reflection loss are all demonstrated by VNA measurements, which are backed by both dielectric and magnetic losses. With high saturation magnetisation, low coercively, and negligible reminisce-properties perfect for attenuating high-frequency electromagnetic waves-VSM analysis validates the composite's soft magnetic nature. This composite is ideal for advanced electromagnetic wave absorbing applications, electromagnetic interference shielding, and stealth technology because of the synergistic combination of magnetic and dielectric loss mechanisms that ensure broadband absorption capability. In environment aspect that can reduce electromagnetic wave pollution in specified area.

REFERENCE:

1. Munk, B. A. (2005). Frequency selective surfaces: theory and design. John Wiley & Sons.
2. An, B. H., Park, B. C., Yassi, H. A., Lee, J. S., Park, J. R., Kim, Y. K., ... & Choi, D. S. (2019). Fabrication of graphene-magnetite multi-granule nanocluster composites for microwave absorption application. Journal of Composite Materials, 53(28-30), 4097-4103.
3. D'Aloia, A. G., Marra, F., Tamburrano, A., De Bellis, G., &Sarto, M. S. (2014). Electromagnetic absorbing properties of graphene–polymer composite shields. Carbon, 73, 175-184.
4. Lagarko AN, Sarychev AK. Electromagnetic properties of composites containing elongated conducting inclusions. Phys Rev B 1996;53:6318–36.
5. De Rosa IM, Mancinelli R, Sarasini F, Sarto MS, Tamburrano A. Electromagnetic design and realization of innovative fiber reinforced broad-band absorbing screens. IEEE Trans EMC 2009;51:700–7.
6. Liu Z, Bai G, Huang Y, Ma Y, Du F, et al. Reflection and absorption contributions to the electromagnetic interference shielding of single-walled carbon nanotube/polyurethane composites. Carbon 2007;45:821–7.
7. Park SH, Thielemann P, Asbeck P, Bandaru PR. Enhanced dielectric constants and shielding effectiveness of, uniformly dispersed, functionalized carbon nanotube composites. ApplPhys Lett 2009;94:243111–3.

8.Al-Saleh MH, Sundararaj U. Electromagnetic interference shielding mechanisms of CNT/polymer composites. Carbon 2009;47:1738–46.
9. Fan Z, Luo G, Zhang Z, Zhou L, Wei F. Electromagnetic and microwave absorbing properties of multi-walled carbon nanotubes/polymer composites. Mater SciEng, B 2006;132(1):85–9.
10. Liu Z, Bai G, Huang Y, Li F, Ma Y, et al. Microwave absorption of single-walled carbon nanotubes/soluble cross-linked polyurethane composites. J PhysChem C 2007;111(37):13696–700.
11. Wang LL, Tay BK, See KY, Sun Z, Tan LK, Lua D. Electromagnetic interference shielding effectiveness of carbon-based materials prepared by screen printing. Carbon 2009;47:1905–10.
12. De Rosa IM, Dinescu A, Sarasini F, Sarto MS, Tamburrano A. Effect of short carbon fibers and MWCNTs on microwave absorbing properties of polyester composites containing nickel-coated carbon fibers. Comp SciTechnol2010;70:102–9.
13. De Rosa IM, Sarasini F, Sarto MS, Tamburrano A. EMC impact of advanced carbon fiber/carbon nanotube reinforced composites for next-generation aerospace applications. IEEE Trans EMC 2008;50:556–63.
14. Liang J, Wang Y, Huang Y, Ma Y, Liu Z, et al. Electromagnetic interference shielding of graphene/epoxy composites. Carbon 2009;47:922–5.
15. Chung DDL. Carbon materials for structural self-sensing, electromagnetic shielding and thermal interfacing. Carbon 2013;50:3342–53.
16. Hsiao ST, Ma CCM,TienHW,LiaoWH,WangYS,etal.Usinga non-covalent modification to prepare a high electromagnetic interference shielding performance graphenenanosheet/ water-borne polyurethane composite. Carbon 2013;60:57–66.
17. Moyseowicz, A., Minta, D., &Gryglewicz, G. (2023). Conductive polymer/graphene-based composites for next generation energy storage and sensing applications. ChemElectroChem, 10(9), e202201145.
18. Aiqiong, W., Li, J., Chen, M., & Zhao, X. (2022). A review of graphene-based broad bandwidth microwave absorbing textile-based composites in the low-frequency range. Journal of Industrial Textiles, 52, 15280837221133113.
19. Bokova ES, Devina EA and Kovalenko GM. Development of multilayer radio-absorbing materials based on nonwoven dielectric matrixes and a polymeric binder. Fibre Chem 2019; 50(5): 462–467.
20. Fu XM, Fan Y, Wang Y, et al. Ultra-wideband microwsave absorber via an integrated metasurface and impedance- matching lattice design. J Phys D-Applied Phys 2019; 52(31): 31LT01.
21. MengFB,WangY,GuoY,etal.Graphene-based microwave absorbing composites: a review and prospective. Composites Part B-Engineering 2018; 137: 260–277.
22. Guo R, Jiang W, Wang L, et al. Core-rim structured carbide MXene/SiO_2 nanoplates as an ultrathin microwave absorber. Carbon 2020; 169: 214–224.
23. Kefeni KK, Msagati TAM and Mamba BB. Ferrite nanoparticles: synthesis, characterisation and applications in electronic device. Mater SciEng B-Advanced Funct Solid-State Mater 2017; 215: 37–55.
24. Tang, L. C., Zhao, L., & Guan, L. Z. (2017). Graphene/polymer composite materials: processing, properties and applications. Advanced composite materials: properties and applications, 349-419.
25. Geim, A. K., &Novoselov, K. S. (2007). The rise of graphene. Nature materials, 6(3), 183-191.
26. Gupta, T. K., Singh, B. P., Singh, V. N., Teotia, S., Singh, A. P., Elizabeth, I., ... &Mathur, R. B. (2014). MnO 2 decorated graphene nanoribbons with superior permittivity and excellent microwave shielding properties. Journal of Materials Chemistry A, 2(12), 4256-4263.
27. Li, X., Yi, H., Zhang, J., Feng, J., Li, F., Xue, D., &Mellors, N. J. (2013). Fe_3O_4–graphene hybrids: nanoscale characterization and their enhanced electromagnetic wave absorption in gigahertz range. Journal of nanoparticle research, 15, 1-11.
28. Mattevi, C.; Kim, H.; Chhowalla, M. A. Review of chemical vapour deposition of graphene on copper. J. Mater. Chem. 2011, 21, 3324.
29. Reina, A.; Jia, X.; Ho, J.; Nezich, D.; Son, H.; Bulovic, V.; Dresselhaus, M. S. and Kong, J. Large area, few-layer graphene films on arbitrary substrates by chemical vapor deposition. Nano Lett. 2009, 9, 30.
30. Sutter, P. W.; Flege, J. I.; and Sutter, E. A. Epitaxial graphene on ruthenium. Nat. Mater. 2008, 7, 406.
31. Hu, C., Lu, T., Chen, F., & Zhang, R. (2013). A brief review of graphene–metal oxide composites synthesis and applications in photocatalysis. Journal of the Chinese Advanced Materials Society, 1(1), 21-39.
32. Si YC, Samulski ET. Exfoliated graphene separated by platinum nanoparticles. Chem Mater. 2008;20:6792.
33. Bell NJ, Ng YH, Du AJ, Coster H, Smith SC, Amal R. Understanding the enhancement in photoelectrochemical properties of photocatalytically prepared TiO_2-reduced graphene oxide composite. J PhysChem C. 2011;115:6004.
34. Huang XD, Zhou XF, Zhou L, Qian K, Wang YH, Liu ZP, Yu CZ. A facile one-step solvo thermal synthesis of SnO_2/graphene nanocomposite and its application as an anode material for lithium-Ion batteries. ChemPhys Chem. 2011;12:278.
35. Koo HY, Lee HJ, Go HA, Lee YB, Bae TS, Kim JK, Choi WS. Graphene-based multifunctional iron oxide nanosheets with tunable properties. ChemEur J. 2011;17:1214.
36. Guo SJ, Dong SJ. Graphene nanosheet: Synthesis, molecular engineering, thin film, hybrids, and energy and analytical applications. ChemSoc Rev. 2011;40:2644.
37. Xiang QJ, Yu JG, Jaroniec M. Graphene-based semiconductor photocatalysts. ChemSoc Rev. 2012;41:782.
38. Huang X, Qi XY, Boey F, Zhang H. Graphene-based composites. ChemSoc Rev. 2012;41:666.

39. Zhang N, Zhang YH, Xu YJ. Recent progress on graphene-based photocatalysts: Current status and future perspectives. Nanoscale. 2012;4:5792.
40. Machado BF, Serp P. Graphene-based materials for catalysis. CatalSci Technol. 2012;2:54.
41. Bai H, Li C, Shi GQ. Functional composite materials based on chemically converted graphene. Adv Mater. 2011;23:1089.
42. Zhu YW, Murali S, Cai WW, Li XS, Suk JW, Potts JR, Ruoff RS. Graphene and graphene oxide: Synthesis, properties, and applications. Adv Mater. 2010;22:3906.
43. Singh, A. P.; Mishra, M.; Sambyal, P.; Gupta, B. K.; Singh, B. P.; Chandra, A.; Dhawan, S. K. Encapsulation of g-Fe_2O_3 Decorated Reduced Graphene Oxide in Polyaniline Core−Shell Tubes as an Exceptional Tracker for Electromagnetic Environmental Pollution. J. Mater. Chem. A 2014, 2, 3581−3593.
44. Belaabed, B., Wojkiewicz, J. L., Lamouri, S., El Kamchi, N., &Lasri, T. (2012). Synthesis and characterization of hybrid conducting composites based on polyaniline/magnetite fillers with improved microwave absorption properties. Journal of Alloys and Compounds, 527, 137-144.
45. Singh, K.; Ohlan, A.; Kotnala, R. K.; Bakhshi, A. K.; Dhawan, S. K. Dielectric and Magnetic Properties of Conducting Ferromagnetic Composite of Polyaniline with γ-Fe_2O_3 Nanoparticles. Mater. Chem. Phys. 2008, 112, 651−658.
46. Kutz M. Handbook of materials selection. Hoboken, NJ: John Wiley&Sons, 2002.
47. Ezrin M. Plastics failure guide: cause and prevention. Munich, Germany: Hanser Publishers, 1996, 473p.
48. Rajendran S, Sivakumar M and Subadevi R. Investigations on the effect of various plasticizers in PVA-PMMA solid polymer blend electrolytes. Mater Lett 2004; 58: 641–649.
49. Nakamura Y, Kariya E, Fukuda T, et al. Glass transition behaviour of PMMA/PVA incompatible blend. PolymPolym Compos 2013; 21: 367–376.
50. Sivakumar M, Subadevi R, Rajendran S, et al. Electrochemical studies on [(1– x)PVA-xPMMA] solid polymer blend electrolytes complexed with LiBF4. Mater ChemPhys 2006; 97: 330–336.
51. Tripathi J, Tripathi S, Sharma A, et al. Effect of PVA concentration on bond modifications in PVA-PMMA blend films. In: AIP conference proceedings, 2016, vol. 1731, pp. 1–3.
52. Sun, X.; He, J.; Li, G.; Tang, J.; Wang, T.; Guo, Y.; Xue, H. Laminated Magnetic Graphene with Enhanced Electromagnetic Wave Absorption Properties. J. Mater. Chem. C 2013, 1 (4), 765−777.
53. Arjmand, M.; Mahmoodi, M.; Gelves, G. A.; Park, S.; Sundararaj, U. Electrical and Electromagnetic Interference Shielding Properties of Flow-Induced Oriented Carbon Nanotubes in Polycarbonate. Carbon 2011, 49 (11), 3430−3440.
54. Qin, F.; Brosseau, C. A Review and Analysis of Microwave Absorption in Polymer Composites Filled with Carbonaceous Particles. J. Appl. Phys. 2012, 111 (6), 061301.
55. da Silva, A. B.; Arjmand, M.; Sundararaj, U.; Bretas, R. E. S. Novel Composites of Copper Nanowire/PVDF with Superior Dielectric Properties. Polymer 2014, 55 (1), 226−234.
56. Adohi, B.; Haidar, B.; Costa, L.; Laur, V.; Brosseau, C. Assessing the Role of Graphene Content in the Electromagnetic Response of Graphene Polymer Nanocomposites. Eur. Phys. J. B 2015, 88, 280.
57. Arjmand, M.; Sundararaj, U. Effects of Nitrogen Doping on Xband Dielectric Properties of Carbon Nanotube/Polymer Nanocomposites. ACS Appl. Mater. Interfaces 2015, 7 (32), 17844−17850.
58. Liang, J.; Wang, Y.; Huang, Y.; Ma, Y.; Liu, Z.; Cai, J.; Zhang, C.; Gao, H.; Chen, Y. Electromagnetic Interference Shielding of Graphene/Epoxy Composites. Carbon 2009, 47 (3), 922−925.
59. Sharif, F., Arjmand, M., Moud, A. A., Sundararaj, U., & Roberts, E. P. (2017). Segregated hybrid poly (methyl methacrylate)/graphene/magnetite nanocomposites for electromagnetic interference shielding. ACS applied materials & interfaces, 9(16), 14171-14179.
60. W.-L. Song, M.-S. Cao, M.-M. Lu, S. Bi, C.-Y. Wang, J. Liu, J. Yuan, L.-Z. Fan, Flexible graphene/polymer composite films in sandwich structures for effective electromagnetic interference shielding, Carbon N. Y., 66 (2014) 67–76.
61. Acharya, S., Ray, J., Patro, T. U., Alegaonkar, P., &Datar, S. (2018). Microwave absorption properties of reduced graphene oxide strontium hexaferrite/poly (methyl methacrylate) composites. Nanotechnology, 29(11), 115605.
62. Fuli Yang, Xingzhe Hou, Lirui Wang, Youjiang Li and Miao Yu,(2020) Preparation of Reduced Graphene Oxide/Magnetic Metal Composites and Its Electromagnetic Wave Absorption Properties, International Conference on Applied Chemistry and Industrial catalysis, IOP Publishing(2020)